nature neuroscience

Intraglomerular inhibition: signaling mechanisms of an olfactory microcircuit

Gabe J Murphy, Daniel P Darcy & Jeffry S Isaacson

Microcircuits composed of principal neuron and interneuron dendrites have an important role in shaping the representation of sensory information in the olfactory bulb. Here we establish the physiological features governing synaptic signaling in dendrodendritic microcircuits of olfactory bulb glomeruli. We show that dendritic γ-aminobutyric acid (GABA) release from periglomerular neurons mediates inhibition of principal tufted cells, retrograde inhibition of sensory input and lateral signaling onto neighboring periglomerular cells. We find that L-type dendritic Ca^{2+} spikes in periglomerular cells underlie dendrodendritic transmission by depolarizing periglomerular dendrites and activating P/Q type channels that trigger GABA release. Ca^{2+} spikes in periglomerular cells are evoked by powerful excitatory inputs from a single principal cell, and glutamate release from the dendrites of single principal neurons activates a large ensemble of periglomerular cells.

The olfactory bulb is a brain region rich in microcircuits that is involved in the early processing of sensory information. Olfactory information is conveyed directly to the brain through conventional synapses in olfactory bulb glomeruli. Here, the axons of olfactory receptor neurons make glutamatergic synaptic contacts with the dendrites of principal neurons, mitral and tufted (M/T) cells and local interneurons called periglomerular neurons[1–3].

Most synaptic interactions within the bulb occur at dendrodendritic synapses. M/T neurons make dendrodendritic synaptic contacts with GABAergic periglomerular neurons in glomeruli (**Fig. 1a**), whereas reciprocal dendrodendritic synapses link M/T lateral dendrites and granule cells in the external plexiform layer[4]. Dendrodendritic synapses between M/T and granule cells provide a basis for self- and lateral inhibition, which is thought to contribute to odor discrimination[5,6]. Dendrodendritic synapses between M/T primary dendrites and periglomerular cells are poised to mediate intraglomerular feedback inhibition and 'gate' M/T cell activity at the first site of olfactory sensory input. In addition, dendrodendritic self-inhibition is thought to have an important role in the temporal patterning of odorant-evoked activity in M/T neurons[7–9].

The mechanisms underlying dendrodendritic signaling between mitral and granule cells in the bulb are beginning to be explored. *N*-Methyl-D-aspartate receptors (NMDARs) are believed to have an important role in triggering GABA release from granule dendrites[10–13]. Ca^{2+} influx through NMDARs has been suggested to trigger GABA exocytosis directly[11,13]. Alternatively, it has been proposed that the slow kinetics of NMDARs are especially good for bringing dendrites to threshold for activating voltage-gated Ca^{2+} channels that trigger release[10,12,14]. Evidence supports a role for high voltage–activated (HVA) N- or P/Q-type channels in dendritic GABA release[14], whereas low voltage–activated (LVA) T-type currents have also been implicated[15].

It is thus unclear whether subthreshold events in interneurons are sufficient to trigger dendrodendritic transmission, or whether strong depolarization provided by Na^+ and/or Ca^{2+} spikes are required for dendritic microcircuits to function under physiological conditions. It is also unclear why brief activation of mitral neurons elicits GABAergic feedback that persists for hundreds of milliseconds. Answering these questions is a critical step toward understanding how the bulb processes and represents information about odorant stimuli. Unfortunately, progress has been hampered by the difficulty in making paired recordings between synaptically coupled cells of the mitral and granule cell layers[14,15].

Several factors suggest that the mechanisms governing signaling between M/T and granule cells are likely to be closely related to those at M/T and periglomerular dendrite contacts. Anatomically, reciprocal synapses formed between glomerular dendritic tufts of M/T cells and dendritic spines of periglomerular cells[1–3] seem virtually identical to dendrodendritic contacts formed between M/T lateral dendrites and granule cells[16]. In addition, NMDAR-mediated excitation of periglomerular cells drives prolonged inhibition of external tufted cells at dendrodendritic synapses in glomeruli, as it does between mitral cells and granule cells in the external plexiform layer[17].

In this study, we take advantage of the convergence of tufted cell and periglomerular cell dendrites within individual glomeruli to identify the fundamental processes that govern synaptic signaling in reciprocal dendrodendritic microcircuits.

RESULTS

Multiple modes of glomerular GABA signaling

We first examined classical reciprocal dendrodendritic inhibition (DDI) in external tufted cells, a class of principal neurons lacking

Neuroscience Graduate Program and Department of Neuroscience, University of California, San Diego, La Jolla, California 92093-0608, USA. Correspondence should be addressed to J.S.I. (jisaacson@ucsd.edu).

Published online 6 February 2005; corrected online 7 February 2005; doi:10.1038/nn1403

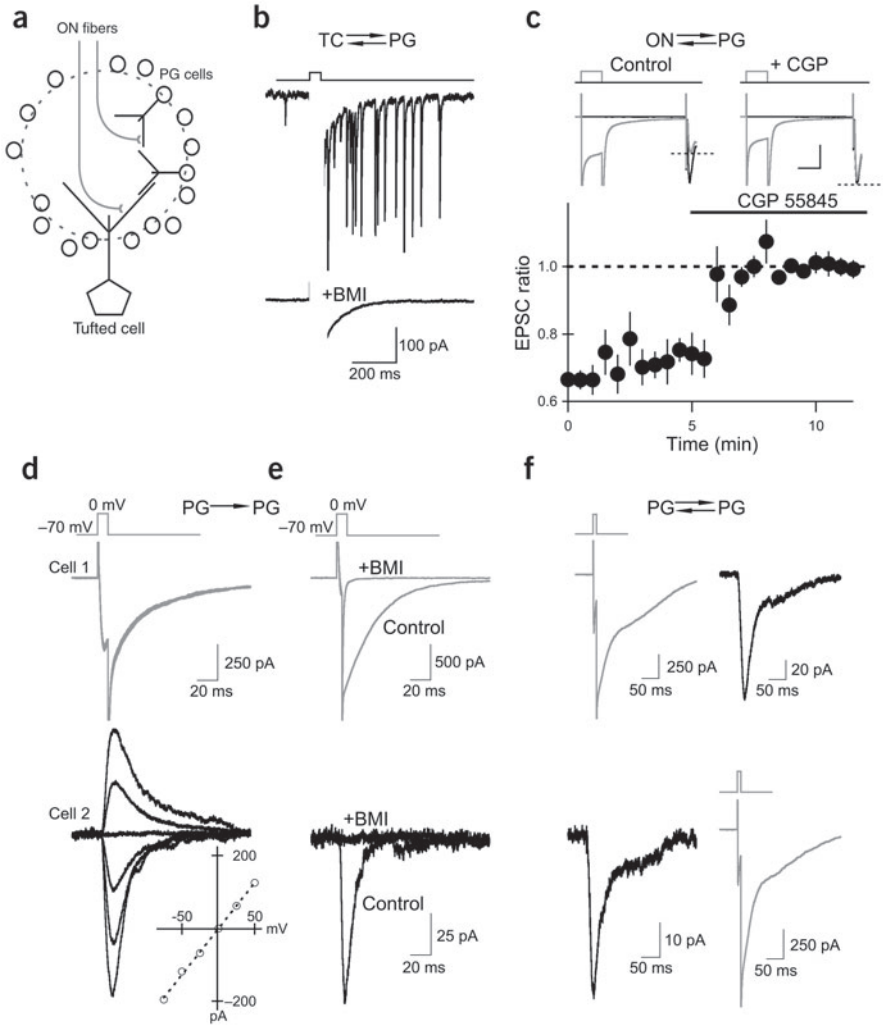

Figure 1 Multiple types of GABAergic signaling in olfactory glomeruli. (**a**) Schematic representation of an olfactory bulb glomerulus. ON, olfactory nerve. (**b**) Tufted cell (TC) dendrodendritic self-inhibition mediated by periglomerular (PG) cells. In the presence of TTX (1 μM), a voltage step (+70 mV, 20 ms) to a TC is followed by a long-lasting barrage of IPSCs that are abolished by the $GABA_A$R antagonist bicuculline (+BMI, 20 μM). (**c**) Retrograde $GABA_B$R-mediated inhibition of sensory input. Top, representative experiment showing that an olfactory nerve–evoked EPSC in a PG neuron is smaller when olfactory nerve stimulation is preceded by a voltage step to cause GABA release (Control, gray trace, dashed line). After CGP 55845 application, the voltage step no longer influences olfactory nerve–evoked EPSC amplitude (+CGP). Bottom, summary of effect of CGP 55845 on the ratio of EPSC amplitudes evoked by olfactory nerve stimulation after a voltage step and olfactory nerve stimulation alone ($EPSC_{step}/EPSC_{con}$; $n = 6$). (**d–f**) Lateral $GABA_A$R-mediated signaling between PG cells. (**d**) A brief (10 ms) voltage step (shown schematically above) in PG cell 1 generates self-inhibition and postsynaptic currents in a neighboring PG neuron (PG cell 2) held at a variety of membrane potentials. Inset, peak postsynaptic current amplitude versus holding potential. (**e**) In another PG pair, self-inhibitory currents in the cell releasing GABA (gray traces) and currents in a neighboring PG neuron (black traces; –70 mV) are abolished by BMI (10 μM). (**f**) Reciprocal signaling between a pair of GABAergic PG neurons.

lateral dendrites that project a single primary dendrite into a nearby glomerulus. To study dendritic transmission, tetrodotoxin (TTX, 1 μM) was added to the artificial cerebrospinal fluid (aCSF) to block Na^+-dependent action potentials. This abolishes the ability of axons to convey action potentials and thus isolates dendritic transmission. Under these conditions, brief (20 ms) activation of tufted cell calcium channels (+70 mV voltage step, CsCl internal) generates a prolonged barrage of synaptic currents mediated through the $GABA_A$ receptor ($GABA_A$R; **Fig. 1b**).

Olfactory nerve terminals express metabotropic $GABA_B$ receptors ($GABA_B$Rs), and $GABA_B$R agonists reduce evoked glutamate release from olfactory nerve terminals onto M/T and periglomerular neurons[18,19]. In addition, application of $GABA_B$R antagonists facilitates olfactory nerve–evoked responses, suggesting that GABA release from periglomerular neurons can mediate diffuse presynaptic inhibition of olfactory nerve transmission[18]. We tested directly whether GABA released from periglomerular neurons acts in a retrograde manner to inhibit glutamate release from olfactory nerve terminals. Periglomerular cells were voltage-clamped using a Cs^+-based internal solution to block any postsynaptic action of $GABA_B$Rs. In the presence of the $GABA_A$R antagonist bicuculline methiodide (BMI, 10–20 μM), olfactory nerve stimulation evoked an excitatory postsynaptic current (EPSC) mediated by AMPA (α-amino-3-hydroxyl-5-methyl-4-isoxazole propionate) receptors in periglomerular neurons[19]. To examine the effect of GABA release from periglomerular neurons on glutamate release from olfactory nerve terminals, we interleaved trials of olfactory nerve stimulation alone with trials in which a depolarizing step (+70 mV) to the periglomerular neuron preceded olfactory nerve stimulation by 75–100 ms (**Fig. 1c**). On average, olfactory nerve–evoked EPSCs in periglomerular neurons were reduced in amplitude by ~30% when olfactory nerve stimulation was preceded by a postsynaptic voltage step; this inhibition was abolished by the $GABA_B$R antagonist CGP 55845 (10 μM; **Fig. 1c**). These data indicate that GABA released from periglomerular cells can act in a retrograde fashion to inhibit glutamate release from olfactory nerve terminals by means of presynaptic $GABA_B$Rs.

GABA release from individual periglomerular neurons can generate self-inhibition by activating $GABA_A$Rs on the same cell[20]. It has also been suggested that dendritically released GABA might generate a $GABA_A$R response in neighboring periglomerular cells through GABA spillover[20]. To examine GABAergic signaling directly between periglomerular cell dendrites, we made simultaneous recordings from pairs of periglomerular neurons that seemed to extend dendrites to a common glomerulus. In the presence of TTX (0.5–1 μM) and glutamate receptor blockers (NBQX, 10 μM, and D-APV, 50 μM, or MK-801, 10 μM), a brief voltage step from –70 to 0 mV in one cell (**Fig. 1d**, cell 1, gray traces) generated a Ca^{2+} current followed by a long-lasting tail current; the tail current reflects dendritically released GABA activating $GABA_A$Rs on the cell from which it was released (self-inhibition[21]).

In many cases, a voltage step that produced self-inhibition in one cell also generated responses in a neighboring unstimulated periglomerular

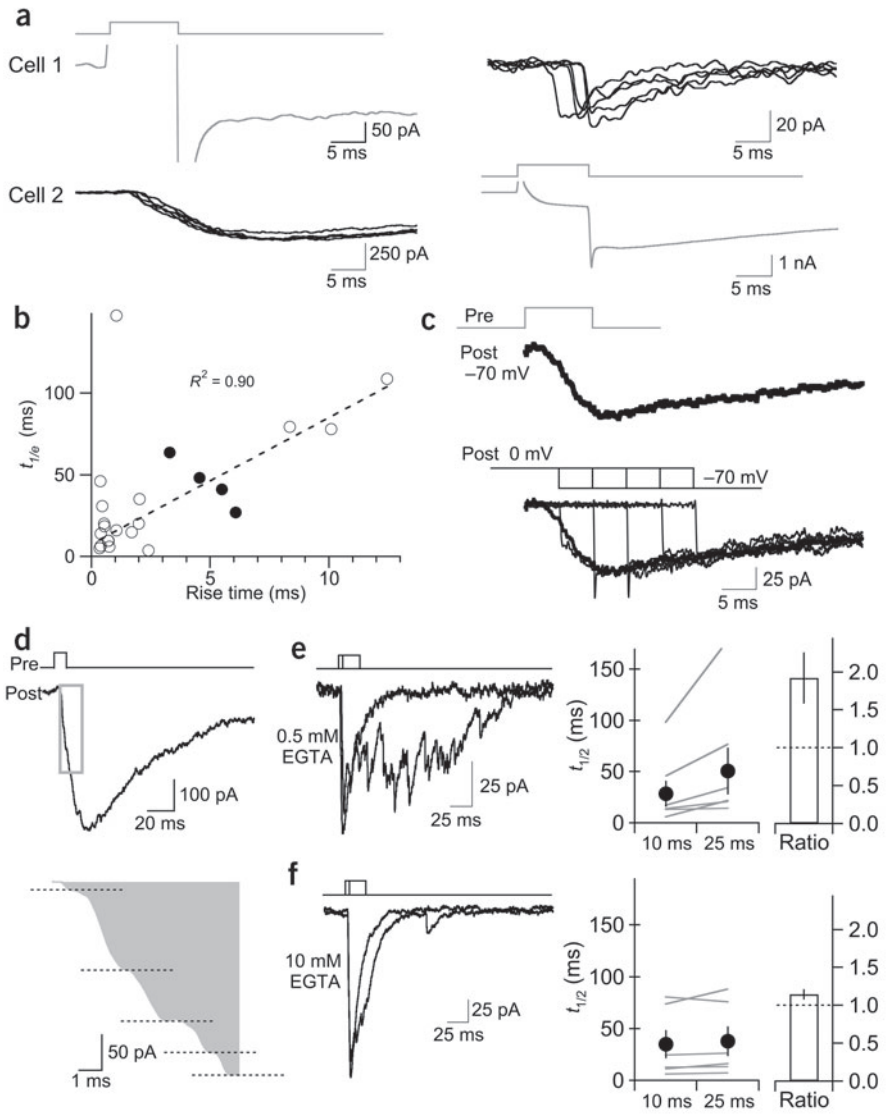

Figure 2 Factors governing the time course of periglomerular signaling. (**a**) Traces from a pair of periglomerular cells in which a voltage step in cell 1 produces self-inhibition and a slow IPSC in a neighboring periglomerular cell; a voltage step in cell 2 produces self-inhibitory currents and fast synaptic currents in cell 1. Five episodes are overlaid in each panel. (**b**) Scatter plot of IPSC decay time (time to 1/*e* of peak) versus 10–90% rise time in 23 paired recordings. The dotted line represents the least-squares linear fit to data from 22 of 23 experiments. Filled circles represent responses tested with voltage jumps. (**c**) Slow $GABA_A$ responses reflect a slow conductance. Top, slow current evoked by a voltage pulse to a neighboring periglomerular cell. Bottom, postsynaptic voltage jumps from 0 to –70 mV at different time points after the presynaptic voltage step. Current is recovered throughout the slow IPSC. (**d**) Slow currents consist of summated asynchronous unitary events. Top, individual sweep showing a slowly rising IPSC. Bottom, blowup of top trace bounded region showing discrete, step-like inflections on the rising phase of the IPSC. (**e**) Increasing the duration of the presynaptic voltage step prolongs the time course of GABA release under control buffering conditions (0.5 mM EGTA). Left, representative experiment showing response to a brief and long depolarizing step. Right, summary of release time course during brief and long presynaptic depolarizations ($n = 6$ pairs). Ratio represents the time course of IPSC charge transfer evoked by 25 ms voltage steps divided by that evoked by a 10 ms voltage step. (**f**) Dialyzing the presynaptic neuron with an internal solution containing 10 mM EGTA prevents prolonged release ($n = 6$ pairs).

neuron (**Fig. 1d**, cell 2). GABA release from one periglomerular cell generated a current in a neighboring periglomerular cell in 25 of 105 paired recordings. In all (25/25) paired recordings where a voltage step in cell 1 generated a current in cell 2, cell 1 showed self-inhibitory currents. The evoked currents in periglomerular cell 2 reversed near the predicted Cl^- reversal potential (0 mV; **Fig. 1d**), suggesting they were due to activation of $GABA_A$Rs. Consistent with this idea, both self-inhibitory currents in cell 1 and the current in cell 2 were blocked by BMI (10–20 μM, $n = 7$; **Fig. 1e**). In approximately one-third of paired recordings where GABA release from cell 1 produced a response in cell 2, a voltage step in cell 2 generated a reciprocal $GABA_A$R-mediated current in cell 1 (**Fig. 1f**). These data provide direct evidence that GABA released from the dendrites of one periglomerular neuron can activate $GABA_A$Rs on neighboring periglomerular neurons.

Is GABA signaling between periglomerular neurons a consequence of GABA spillover or is it due to synaptic signaling? To address this issue, we examined the kinetics of currents produced by signaling between periglomerular cells. We found that currents evoked in one periglomerular neuron after GABA release from another could show very rapid rise times (~1 ms; **Fig. 2a**). Indeed, in most (16/23) cases (**Fig. 2b**), unitary currents evoked in one periglomerular cell by GABA released from another periglomerular cell showed rise times resembling those at GABAergic synapses[12,21]. These data suggest that periglomerular neurons can communicate with each other through dendrodendritic synaptic contacts because the rise times of inhibitory postsynaptic currents (IPSCs) evoked by dendritic GABA release from one periglomerular neuron onto another are too fast to be accounted for by anything other than direct synaptic signaling.

Signaling between most periglomerular neurons showed kinetics reminiscent of synaptic communication, but GABA release from one periglomerular neuron onto another did not always produce fast, unitary, $GABA_A$R-mediated currents. In some pairs, the rise times of evoked responses were >5 ms, and there seemed to be a correlation between the rise and decay time of the events (**Fig. 2b**). To examine whether electrotonic filtering of synapses at distant dendritic sites slowed IPSC kinetics, we used a voltage jump protocol[22,23] to determine the time course of the underlying conductance in cases where currents had slow (3–7 ms) rise times (**Fig. 2b**, filled circles). In every instance ($n = 4$), the time course of the current recovered from voltage jumps matched that obtained at –70 mV, indicating that the slow kinetics of the response reflect a slow underlying conductance (**Fig. 2c**). These data indicate that the slow kinetics of some $GABA_A$R-mediated currents in periglomerular cells cannot be due to dendritic filtering of fast synaptic conductances.

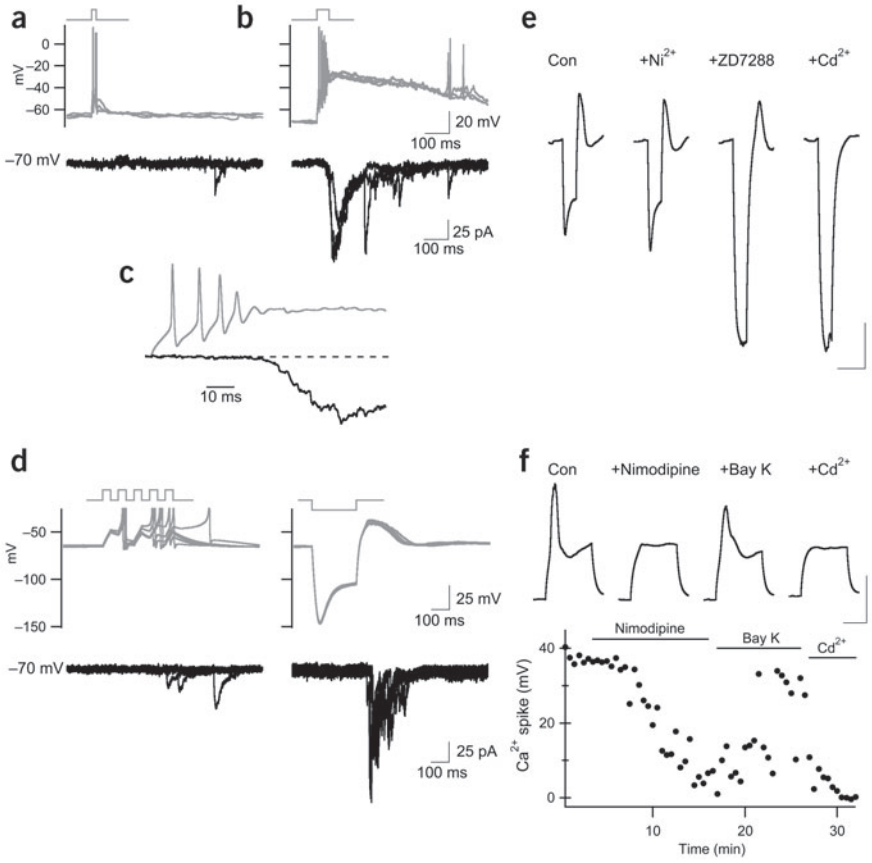

Figure 3 Ca^{2+} spikes mediated by dihydropyridine-sensitive channels are more effective triggers of periglomerular GABA release than fast Na^+ spikes. (**a**) A brief current step in the presynaptic neuron (gray traces, KCl internal) evoked Na^+ spikes but no IPSC in the postsynaptic cell (black traces, CsCl internal). (**b**) A slightly longer current step generates Na^+ spikes and a subthreshold depolarization in the presynaptic neuron, and a barrage of IPSCs in the postsynaptic cell. Three consecutive trials are superimposed in each panel. (**c**) Blowup of a single trial in **b**. (**d**) Another paired recording where a train of action potentials (gray traces, KCH_3SO_4 internal) occasionally evoked an IPSC. In contrast, the subthreshold depolarization after a hyperpolarizing current step evoked robust release in the presence of TTX. Five traces are superimposed. (**e**) The subthreshold depolarization after a hyperpolarizing current step is insensitive to Ni^{2+} (100 μM) and ZD7288 (25–50 μM), but is blocked by 100 μM Cd^{2+}. (**f**) Nimodipine blocks Ca^{2+} spikes evoked by a small (15 pA) depolarization from rest (~–70 mV) in the presence of TTX, Ni^{2+} and ZD7288. Application of Bay K 8664 (10 μM; Bay K) recovered the spike. The time course of the experiment is shown below. Scale bars in **e** and **f**: 25 mV, 500 ms.

Buffer saturation governs the duration of GABA release

Slow $GABA_AR$ synaptic responses between periglomerular cells may indicate a diffuse, spillover form of transmission, or a postsynaptic feature such as $GABA_ARs$ with intrinsically slow kinetics. However, inspection of the rising phase of individual slow currents revealed discrete, step-like transitions (**Fig. 2d**). These current steps suggest that the slow rise of some responses may reflect the summation of asynchronous unitary events with fast rise times. We next took advantage of the good success rate of recording from synaptically coupled periglomerular cell pairs to explore further the factors shaping the time course of dendritic release.

A puzzling feature of DDI between M/T cells and local interneurons is the prolonged duration of asynchronous IPSCs after M/T cell glutamate release[10–12,17]. In periglomerular paired recordings, we found that the time course of release was dependent on the duration of the presynaptic stimulus (**Fig. 2e**). Increasing the duration of the presynaptic voltage step from ≤10 ms to ≥20 ms greatly prolonged the duration of dendritic GABA release. We quantified the time course of release by calculating the time it took for half of the postsynaptic charge transfer to occur after the end of the presynaptic voltage step. Increasing the duration of the presynaptic voltage step nearly doubled the time it took for half of the charge transfer to occur after cessation of the presynaptic depolarization (**Fig. 2e**). Prolonged release evoked by a ≥20 ms step was abolished when the presynaptic neuron was dialyzed with an internal solution containing a high concentration of the Ca^{2+} chelator EGTA (10 mM; **Fig. 2f**). These results indicate that prolonged, asynchronous, dendritic GABA release can, in part, reflect the saturation of endogenous Ca^{2+} buffers in the presynaptic cell.

Dominant role for dendritic Ca^{2+} spikes in GABA release

To explore dendritic GABA release under more physiological conditions, we carried out experiments in which the presynaptic periglomerular neuron was held in a current clamp. To our surprise, single action potentials generated by a brief presynaptic depolarizing current step (20–50 pA, 10 ms) generally failed to evoke an IPSC in postsynaptic periglomerular cells or tufted cells (**Fig. 3a**). In these same experiments, slightly longer current steps often triggered a burst of action potentials and a long-lasting, subthreshold depolarization that generated a barrage of IPSCs in the postsynaptic cell (**Fig. 3b**). Most GABA release generally occurred well after the last Na^+ spike and coincided with the onset of the slow depolarization (**Fig. 3c**). Although single action potentials were relatively ineffective triggers of GABA release, IPSCs were more routinely observed during trains of action potentials (**Fig. 3d**). In these same cells in which action potentials were ineffective triggers of release, IPSCs were readily evoked in the presence of TTX by long-lasting (>100 ms) subthreshold depolarizations that followed a hyperpolarizing current step ($n = 5$; **Fig. 3d**). The marked differences in transmission evoked by action potentials as compared to slow depolarizations were consistently observed whether the postsynaptic cell was a tufted cell ($n = 7$) or another periglomerular neuron ($n = 16$; **Supplementary Fig. 1** online).

What underlies these slow depolarizations, and why are they such effective triggers of dendritic GABA release? We first studied the rebound depolarizations triggered by hyperpolarizing current injection. In the presence of TTX, rebound depolarizations were insensitive to nickel (100 μM; **Fig. 3e**), an inorganic blocker of LVA T-type Ca^{2+} channels[24]. In agreement with previous studies, we saw a hyperpolarization-activated cation conductance in a large fraction of periglomerular cells[25,26]. The I_h channel blocker ZD7288 (25–50 μM) blocked the depolarizing sag during hyperpolarizing current injection, but did not abolish the rebound depolarization (**Fig. 3e**). In the presence of Ni^{2+} and ZD7288, the nonselective Ca^{2+} channel blocker Cd^{2+} (100 μM)

abolished the rebound potential ($n = 5$). These data suggest that non-T-type Ca^{2+} channels mediate subthreshold depolarizations in periglomerular cells.

In a variety of central neurons, subthreshold depolarizations reflect dendritic Ca^{2+} spikes that propagate passively to the soma[27–30]. Similar to these neurons with active dendrites, periglomerular neurons seem to generate dendritic Ca^{2+} spikes that we record in the soma as an attenuated subthreshold potential. We next explored the Ca^{2+} channels underlying dendritic Ca^{2+} spikes in periglomerular neurons. Ca^{2+} spikes persisted in the presence of Ω-conotoxin MVIIC (5 μM, $n = 3$) or Ω-agatoxin IVA (250 nM, $n = 3$), ruling out a role for N-, P- or Q-type Ca^{2+} channels. However, the L-type Ca^{2+} channel antagonist nimodipine (20 μM) largely abolished Ca^{2+} spikes evoked by small (5–15 pA) depolarizations ($n = 5$; **Fig. 3f**) or hyperpolarizing current injection ($n = 3$; data not shown). Application of the dihydropyridine agonist Bay K 8644 (5–10 μM) rescued the Ca^{2+} spike after application of nimodipine ($n = 4$; **Fig. 3f**). These data indicate that L-type channels are most likely to underlie dendritic Ca^{2+} spikes in periglomerular cells.

Although periglomerular neurons are electrotonically compact, it is possible that Na^+-dependent action potentials do not propagate well enough through periglomerular dendrites to cause appreciable Ca^{2+} influx to trigger release. To address this possibility, we filled cells with fluorescent Ca^{2+}-indicator dye (Oregon Green BAPTA-1, 100 μM) to examine dendritic Ca^{2+} transients (**Fig. 4**). Action potentials evoked Ca^{2+} transients throughout the dendritic tree (>20 μm from the soma) of every periglomerular neuron examined. In a segment of dendrite that is ~25 μm from the soma of a periglomerular neuron, a train of five action potentials at 40 Hz generated a Ca^{2+} transient throughout the dendritic compartment (**Fig. 4a**). This transient was much smaller than that evoked by a rebound Ca^{2+} spike (**Fig. 4b**). Although the Ca^{2+} transients evoked by trains of action potentials were abolished by TTX (data not shown), the large transient evoked by the Ca^{2+} spike persisted (**Fig. 4c**).

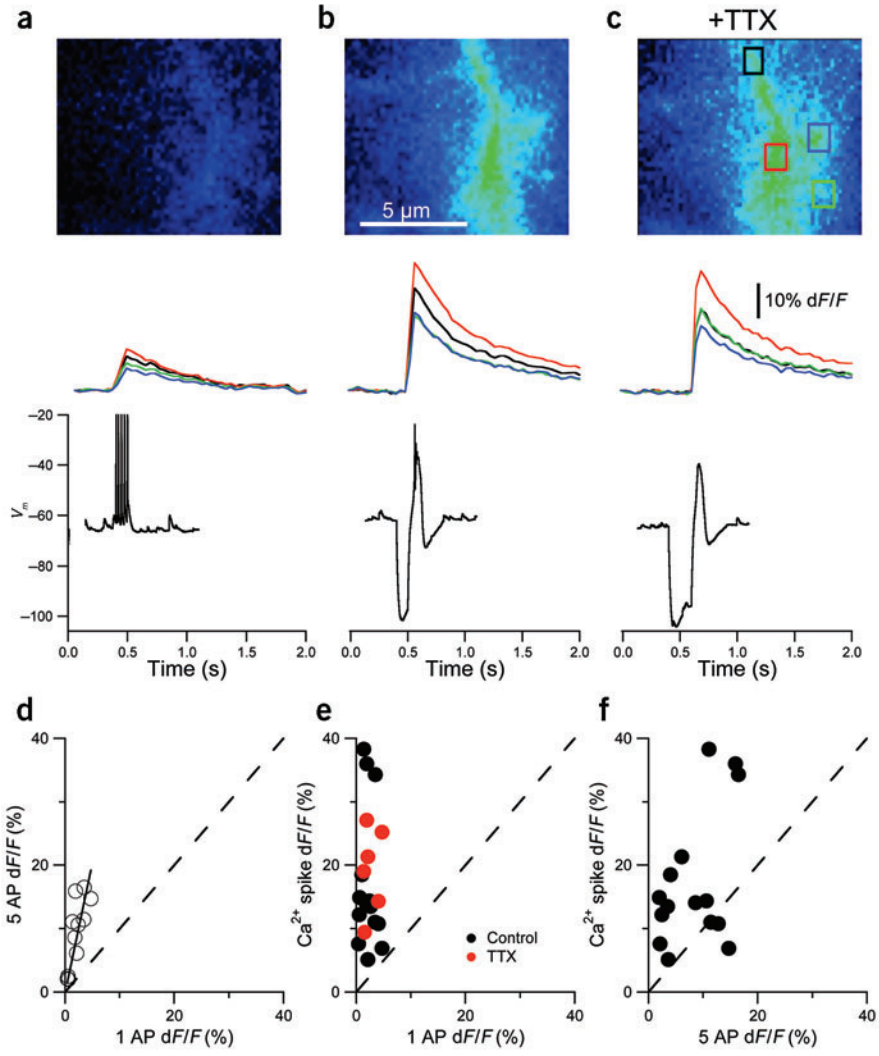

Figure 4 Ca^{2+} spikes generate more Ca^{2+} influx than action potentials in periglomerular dendrites. (**a**–**c**) Pseudocolor images in the top row reflect peak Ca^{2+} in a segment of periglomerular dendrite in response to a brief train of action potentials (**a**), and a rebound Ca^{2+} spike under control conditions (**b**) and in the presence of TTX (**c**). Images are mapped on the same intensity scale. Colored boxes in **c** represent approximate regions of interest used to calculate d*F*/*F* shown in the second row. (**d**) Comparison of Ca^{2+} transient amplitudes produced by trains of five action potentials at 10–40 Hz versus single action potentials in the same cells. Solid line is a least-squares fit with slope = 4.1. AP, action potential. (**e**) Ca^{2+} influx produced by Ca^{2+} spikes under control conditions (black circles, $n = 15$) and in the presence of TTX (red circles, $n = 5$) is much larger than that produced by single action potentials in the same cells. (**f**) Dendritic Ca^{2+} spikes generally produce more Ca^{2+} influx than trains of five action potentials.

On average, single action potentials generated a peak change in the fluorescence over baseline fluorescence (d*F*/*F*) of 2.1 ± 0.3% ($n = 16$ cells). Trains of five action potentials at 10–40 Hz produced a peak transient of 9.2 ± 1.6% ($n = 11$ cells). The transient evoked by five action potentials was nearly the linear sum of that produced by a single action potential in the same cells (**Fig. 4d**). The peak transient evoked by a Ca^{2+} spike (d*F*/*F* = 16.8 ± 2.6%, $n = 15$) always greatly exceeded that generated by a single action potential (**Fig. 4e**), and generally was larger than that evoked by trains of five action potentials (**Fig. 4f**). These results indicate that Ca^{2+} spikes produce much greater Ca^{2+} influx into periglomerular dendrites than action potentials.

LVA L-type current in periglomerular cells

What channels underlie the generation of low-threshold Ca^{2+} spikes in periglomerular dendrites? We found that low-threshold spikes are sensitive to dihydropyridines and can be evoked in the presence of ZD7288 and 100 μM nickel. We next considered the possibility that L-type channels may be active near the resting membrane potential of periglomerular cells. In current clamp recordings, we observed that long (400 ms) hyperpolarizing current steps to –100 mV reduced dendritic Ca^{2+} before the generation of a rebound spike (**Fig. 5a,b**), and the decrease was correlated with the resting potential ($n = 10$ cells; **Fig. 5c**). This voltage-sensitive reduction in resting

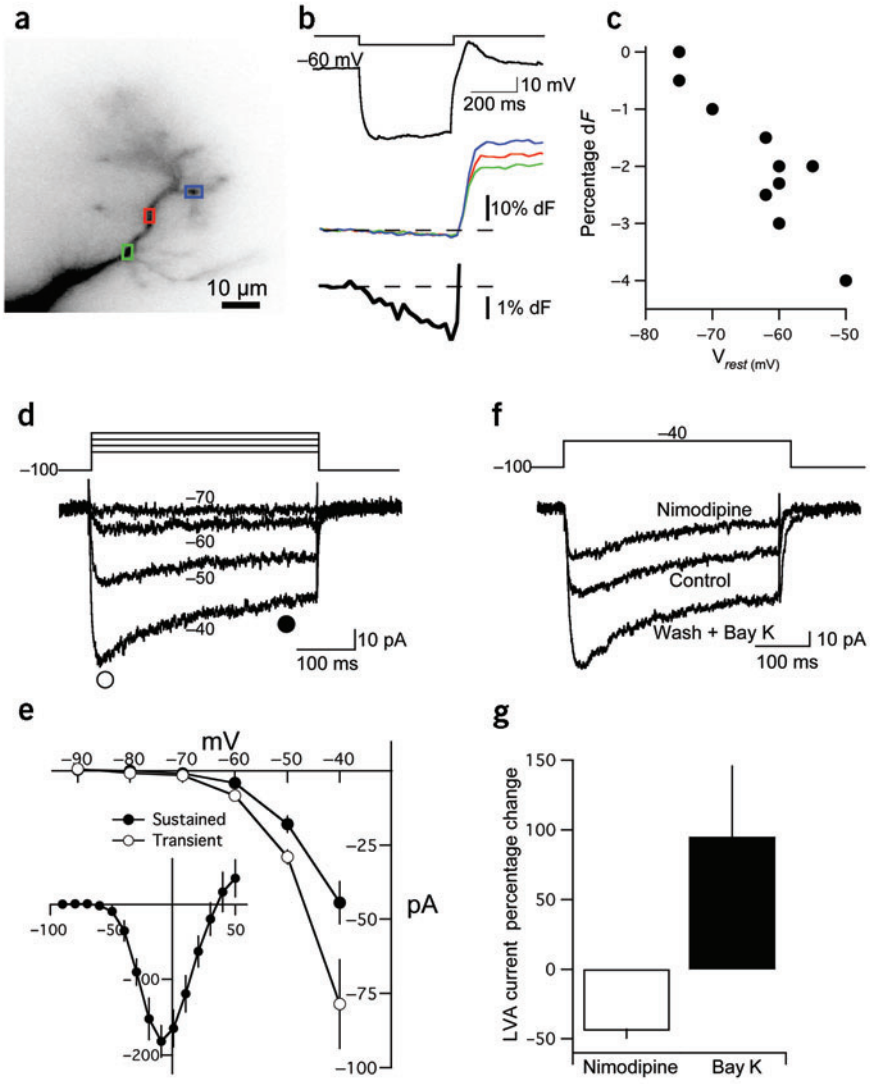

Figure 5 Low voltage–activated dihydropyridine sensitive Ca^{2+} currents in periglomerular cells. (**a–c**) Hyperpolarization reduces resting Ca^{2+} in periglomerular dendrites. (**a**) Image of a periglomerular dendrite. (**b**) Top, a long hyperpolarizing current step from rest (–60 mV) generates a rebound Ca^{2+} spike. Middle, changes in calcium in the three regions outlined in **a**. Bottom, average of the three regions shown above on an expanded scale. (**c**) Plot of the change in calcium level (dF) evoked at the end of a 400 ms hyperpolarizing step to approximately –100 mV versus membrane potential for ten cells. (**d–g**) Sustained low voltage–activated Ca^{2+} currents in periglomerular cells. (**d**) Response of a typical cell to voltage steps (V_{hold} = –100 mV) from –70 mV through –40 mV. Symbols represent the time points used to measure the transient (open circle) and sustained (filled circle) components of Ca^{2+} currents. (**e**) *I/V* relationship for LVA sustained and transient current in periglomerular cells (n = 8 cells). Inset, full *I/V* of the sustained current (n = 4 cells). (**f**) Single experiment showing calcium currents under control conditions, in the presence of nimodipine (20 µM) and after washout of nimodipine in the presence of Bay K 8644 (5 µM; Bay K). (**g**) Summary of effects of nimodipine (n = 7) and Bay K 8644 (n = 4) on currents evoked by voltage steps to –40 and –50 mV, respectively.

Ca^{2+} suggests that voltage-gated Ca^{2+} channels can be active near the resting membrane potential.

We next studied directly Ca^{2+} currents in voltage-clamped periglomerular cells (V_{hold} = –100 mV). Voltage steps evoked sustained Ca^{2+} currents that activated near the resting membrane potential of periglomerular cells (~–60 mV; **Fig. 5d,e**). We did not find substantial T-type currents in periglomerular cells. The sustained LVA current was blocked by nimodipine (–44.1 ± 5.7% change, n = 7) and potentiated by Bay K 8644 (+95 ± 50% change, n = 4; **Fig. 5f,g**). These properties are consistent with reports of LVA L-type channels in suprachiasmatic neurons[31] and pyramidal neurons of the hippocampus[32,33] and amygdala[34]. These findings suggest that L-type Ca^{2+} channels can be active near the resting potential of periglomerular neurons.

The effects of nimodipine on dendritic Ca^{2+} spikes and Ca^{2+} currents in periglomerular neurons prompted us to examine the role of L-type channels in DDI between tufted cell and periglomerular neurons. In the presence of TTX, nimodipine (20 µM) caused a reduction in DDI (53 ± 15% of control) that was restored by the subsequent application of Bay K 8644 (5 µM, n = 5; **Fig. 6a**). We next carried out the identical experiment in cells bathed with a low Mg^{2+} (100 µM) aCSF. This facilitates DDI by enhancing the activation of interneuron NMDARs[10–12,17]. Under these conditions, nimodipine also caused a reduction in DDI (69 ± 7% of control) that was recovered by Bay K 8644 (n = 4; **Fig. 6a**). These experiments indicate that L-type calcium channels contribute to DDI under physiological conditions as well as under conditions in which the contribution of NMDARs is greatly enhanced.

Ca^{2+} channels coupled to GABA exocytosis

Do dihydropyridines act on the channels directly coupled to release from tufted cell or periglomerular cells? We first explored the possibility that the action of nimodipine on DDI reflected a block of the calcium channels governing glutamate release from tufted cells. We measured tufted cell glutamate release by recording self-excitation in low Mg^{2+} aCSF supplemented with picrotoxin (100 µM) to block $GABA_A$Rs. Under these conditions, the cell is held at –60 mV and a voltage step to 0 mV is followed by a tail current owing to activation of NMDARs on the same cell[35–37]. Nimodipine (20 µM) had no effect on self-excitation (n = 6; **Fig. 6b**), ruling out a role for L-type channels in tufted cell glutamate release.

We next focused on the properties of Ca^{2+} channels governing dendritic GABA release by recording from synaptically coupled periglomerular cell pairs. We studied the voltage dependence of dendritic transmission by stepping the presynaptic neuron to membrane potentials between –70 and +50 mV from a holding potential of –90 mV. Only steps that were sufficiently large to activate HVA Ca^{2+} channels (>–40 mV) evoked an IPSC in synaptically coupled neurons (**Fig. 6c**). These data demonstrate that, like conventional nerve terminals, Ca^{2+} influx through HVA Ca^{2+} channels triggers dendritic GABA release from periglomerular neurons.

We used $GABA_A$R-mediated self-inhibition to characterize the calcium channels directly coupled to GABA release from periglomerular

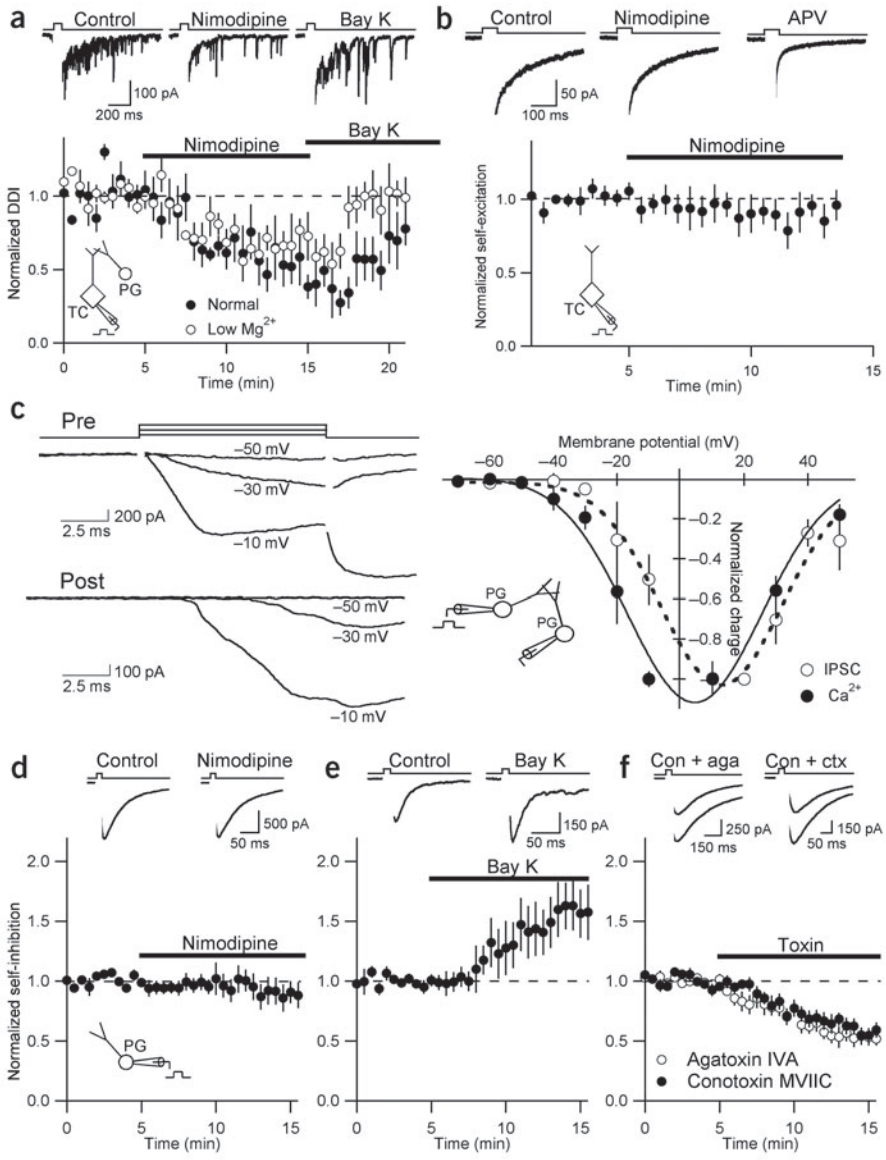

Figure 6 L-type Ca^{2+} channels are required for tufted cell–periglomerular cell (TC-PG) dendrodendritic inhibition but are not normally coupled to exocytosis. (**a**) DDI in a TC is reduced by nimodipine (20 μM) and recovered by Bay K 8644 (5 μM; Bay K). Summary plot shows dendrodendritic inhibition in normal aCSF (filled circles) and low Mg^{2+} aCSF (open circles). Top traces, representative TC recording showing reduction and recovery of dendrodendritic inhibition. (**b**) L-type Ca^{2+} channels do not contribute to TC glutamate release. Top traces, nimodipine has no effect on TC self-excitation in a representative cell. Subsequent application of APV (50 μM) abolishes the response. (**c**) Left, presynaptic PG Ca^{2+} current generated by voltage steps from –90 to –50, –30 and –10 mV and postsynaptic responses in a neighboring cell. Right, normalized Ca^{2+} current (filled circles) and IPSC charge (open circles) versus the presynaptic membrane potential from eight PG-PG pairs. Each point represents the average of three to eight experiments. Ca^{2+} currents were normalized to the response at –10 mV; IPSC charge was normalized to the response at +10 mV. IPSC charge was measured only during the step to exclude responses resulting from Ca^{2+} tail currents. (**d**) Nimodipine (20 μM) has no effect on PG self-inhibition. Top traces, bicuculline-subtracted records from a representative PG. (**e**) Bay K 8644 (5 μM) enhances PG self-inhibition. Top traces, bicuculline-subtracted traces from a representative cell. (**f**) In separate experiments, both agatoxin IVA (1 μM) and conotoxin MVIIC (5 μM) reduce PG self-inhibition. Top traces, representative PGs showing bicuculline-subtracted responses under control conditions (Con) and in the presence of agatoxin IVA (aga) or conotoxin MVIIC (ctx).

dendrites. Nimodipine (20 μM) did not affect self-inhibition in periglomerular cells ($n = 9$; **Fig. 6d**), indicating that Ca^{2+} influx through L-type channels is not normally coupled to GABA release. Curiously, application of Bay K 8644 (5 μM) led to an increase in self-inhibition (160 ± 21% of control, $n = 8$; **Fig. 6e**). This indicates that although L-type channels do not normally support exocytosis, facilitating L-type channels allows them to act as a source of calcium for GABA release. The selective N-type blocker Ω-conotoxin GVIA (5 μM) did not affect self-inhibition ($n = 5$), suggesting that N-type channels are not involved in GABA release. However, Ω-conotoxin MVIIC (5 μM), a blocker of N- and P/Q type channels, caused a reduction in self-inhibition (**Fig. 6f**, 58 ± 6% of control, $n = 8$). In separate experiments, the P/Q antagonist agatoxin IVA (1 μM) reduced self-inhibition by an almost identical amount (**Fig. 6f**, 53 ± 7% of control, $n = 6$). Pretreatment of slices with nimodipine (20 μM) did not augment the action of the toxins, and results with and without the antagonist were pooled. These results suggest that P/Q-type calcium channels have a major role in triggering dendritic GABA release.

To confirm the role of P/Q-type channels in triggering GABA release from periglomerular dendrites, we used caged calcium to evoke DDI in tufted cells. This approach triggers glutamate release from tufted cell dendrites, but bypasses the need for tufted cell dendrite Ca^{2+} channels during DDI[14]. Photolysis of caged Ca^{2+} in tufted cells evoked a barrage of IPSCs similar to those evoked by depolarizing voltage steps in the same cell (**Supplementary Fig. 2** online). Recordings from slices treated with Ω-conotoxin MVIIC (5 μM) and agatoxin IVA (500 nM) were interleaved with naive slices as a control. In control slices, DDI evoked by voltage steps averaged 431 ± 84 pA•s ($n = 7$), whereas in toxin-treated slices the charge transfer was markedly less (84 ± 42 pA•s, $n = 10$). DDI evoked by photolysis of caged Ca^{2+} in the same control slices was 145 ± 53 pA•s, whereas the response in toxin-treated slices was much smaller (33 ± 19 pA•s; **Supplementary Fig. 2** online). These results indicate the important role of P/Q-type channels in periglomerular GABA release during dendrodendritic synaptic signaling.

Strong impact of single principal cells within glomeruli

What is the impact of a single principal cell on interneurons in glomerular microcircuits? To address this question, we loaded slices with the cell-permeable calcium indicator Oregon Green BAPTA-1 AM (10 μM). We recorded from tufted cells in a voltage clamp using a

KCl-based internal solution. Trains of brief depolarizations (+80 mV, 3 ms, 10 ms ISI) were used to evoke action currents (action potentials) to drive self-inhibition. Activation of a tufted cell generated robust calcium transients in small (<10 μm diameter), round compartments surrounding the glomerulus to which the tufted cell projected a dendritic tuft (**Fig. 7a**). The size and location of these fluorescent puncta are consistent with the cell bodies of periglomerular cells. Indeed, in targeted whole-cell recordings (9/9 cells; **Supplementary Fig. 3** online), the calcium transients always occurred in cells that showed hallmarks of periglomerular neurons (that is, input resistance ≥1 GΩ, self-inhibition, calcium spikes).

Activation of periglomerular cells coincided with the onset of tufted cell DDI (**Fig. 7b**). Single tufted cells activated multiple periglomerular cells in every glomerulus examined (5 ± 1 periglomerular cells, range = 2–7, $n = 8$ glomeruli). Although the number of periglomerular cells activated on individual trials varied with the magnitude of DDI, tufted cells reliably recruited the same ensemble of interneurons. An example of this is shown (**Fig. 7c–e**). We first stimulated a tufted cell with a short pulse train (five action potentials) that was just at threshold for eliciting DDI. On one trial, this stimulus activated seven periglomerular cells during and immediately after the pulse train (**Fig. 7c**). The DDI in this trial showed both an early, relatively synchronous component and delayed IPSCs. The next trial using the same brief stimulus activated only one periglomerular cell and did not elicit substantial DDI (**Fig. 7d**). Increasing the stimulus to ten action potentials activated the same ensemble of periglomerular cells observed in the first trial and produced a prolonged barrage of IPSCs in the tufted cell (**Fig. 7e**). These results indicate that single tufted cells can reliably recruit the same ensemble of periglomerular cells. In addition, the kinetics of periglomerular cell activation (**Fig. 7b–e**) reveal considerable temporal variability (jitter) that overlaps with the time course of DDI. Similar results were obtained when DDI was evoked in the presence of TTX (**Supplementary Fig. 3** online).

The somatic Ca^{2+} transients evoked in periglomerular cells suggest that the dendrite of a single principal cell has a powerful impact on individual interneurons. To explore the strength of this microcircuit, we made recordings from pairs of synaptically coupled periglomerular and external tufted cells in the presence of TTX. In a typical experiment, a brief depolarizing step in the voltage-clamped tufted cell generated a large excitatory postsynaptic potential (EPSP) in the periglomerular neuron (**Fig. 8a**). On average, tufted cell glutamate release produced a 10.8 ± 1.5 mV EPSP in periglomerular neurons (V_m ~–65 mV, $n = 14$). In 7 of 14 tufted cell–periglomerular cell pairs, the EPSP was followed by an all-or-none Ca^{2+} spike that showed kinetics nearly identical to the rebound Ca^{2+} spike after a hyperpolarizing step in the same cell (**Fig. 8b**). APV (50 μM) had no effect on the rebound Ca^{2+} spike, but abolished the spike driven by glutamate release from the tufted cell (**Fig. 8a**, $n = 3$) and greatly reduced dendrodendritic self-inhibition. These data demonstrate that glutamate release from a single principal cell can trigger a dendritic Ca^{2+} spike in periglomerular cells. Moreover, these data suggest that NMDARs are critical for dendritic Ca^{2+} spike generation.

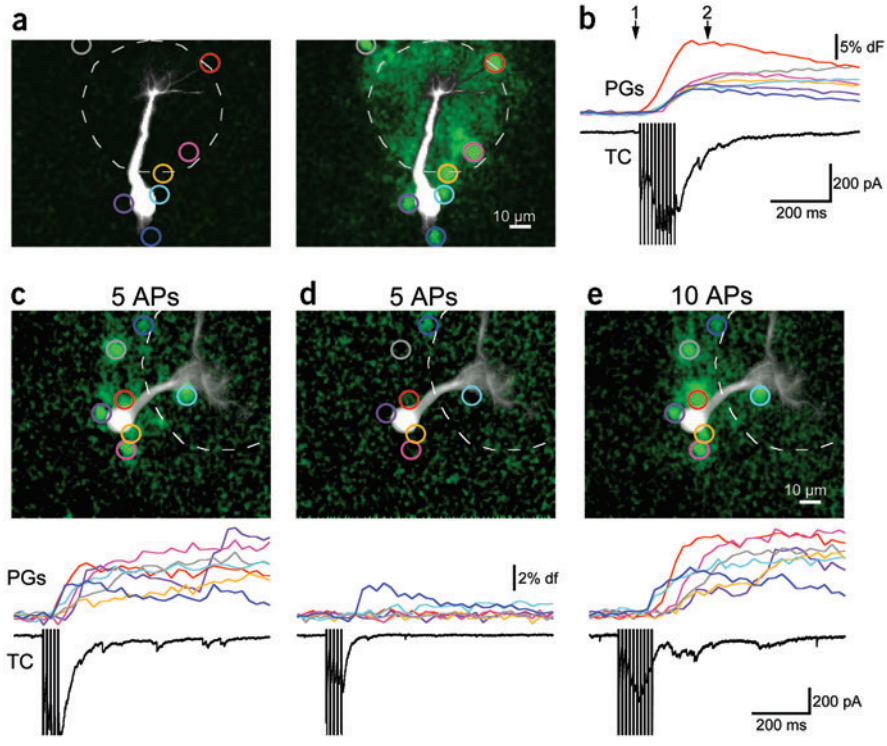

Figure 7 Individual tufted cells (TCs) activate an ensemble of periglomerular (PG) cells. (**a**) Images of an intracellularly recorded TC (white) and Ca^{2+} indicator–loaded PG cells (colored circles) before (left) and after (right) a train of ten action currents (APs). (**b**) Ca^{2+} transients in PG cells shown in **a** and dendrodendritic inhibition evoked in the TC. Arrows indicate frames shown in **a**. (**c–e**) PG cell activation covaries with dendrodendritic inhibition. Top, images of peak PG cell activity evoked by TC stimulation at threshold for eliciting dendrodendritic inhibition. Bottom, time course of TC responses and PG calcium transients. A DIC image was used to estimate the position of the glomerulus (dashed circle). Displayed images were median filtered and level adjusted.

In vivo, respiration generates rhythmic sensory input to the olfactory bulb[8,9,38] and M/T cells are entrained by theta frequency olfactory nerve stimulation *in vitro*[39,40]. We next tested whether rhythmic activity in a tufted cell was sufficient to generate spikes in synaptically coupled periglomerular neurons. In current clamp, tufted cells fired bursts of action potentials in response to sinusoidal current injection (2 Hz; 100–200 pA). Single action potentials in a tufted cell generated a large (8.3 ± 1.7 mV, $n = 12$ pairs) EPSP in synaptically coupled periglomerular neurons, and theta-patterned bursts in tufted cells led to a complex Na^+/Ca^{2+} spike in periglomerular neurons in 6 of 12 paired recordings (**Fig. 8c**). Tufted cell activity was most effective at bringing periglomerular neurons to threshold during the first theta cycle. The dynamic nature of tufted cell input was apparent from analyzing tufted cell–evoked depolarizations in periglomerular neurons as a function of the theta cycle; the second to fourth theta cycles in the tufted cell produced a much smaller depolarization in periglomerular neurons than the first theta cycle ($n = 9$; **Fig. 8c**, inset). These results demonstrate that physiologically relevant patterns of activity in tufted cells can produce large depolarizations in periglomerular cells that are sufficient to evoke Ca^{2+} spikes. In addition, these data indicate that the impact of tufted cells on periglomerular neurons is dynamic during rhythmic patterns of activity like those observed *in vivo*.

DISCUSSION

Here we have established key physiological features of the microcircuit underlying intraglomerular inhibition. First, we found that, in addition to mediating dendrodendritic $GABA_AR$ inhibition onto principal neurons, periglomerular cells make dendrodendritic synaptic contacts onto each other. Periglomerular dendrite GABA release also produces retrograde inhibition of sensory input through presynaptic $GABA_BRs$. Second, we exploited the favorable electrotonic properties of periglomerular neurons to study the relationship between Ca^{2+} influx and dendritic GABA release in detail. We found that transmitter release from periglomerular dendrites requires Ca^{2+} influx through P/Q-type Ca^{2+} channels. Under physiological conditions, dendritic release is triggered much more effectively by Ca^{2+} spikes than Na^+-dependent action potentials. We showed that L-type Ca^{2+} channels mediate dendritic Ca^{2+} spikes in periglomerular neurons but do not normally couple to exocytosis. Third, we examined the network properties underlying signaling between principal cells and glomerular interneurons. We showed that glutamate release from a single principal cell is sufficiently powerful to generate dendritic Ca^{2+} spikes in periglomerular cells. In addition, excitation from one principal cell dendrite activates a large ensemble of periglomerular cells.

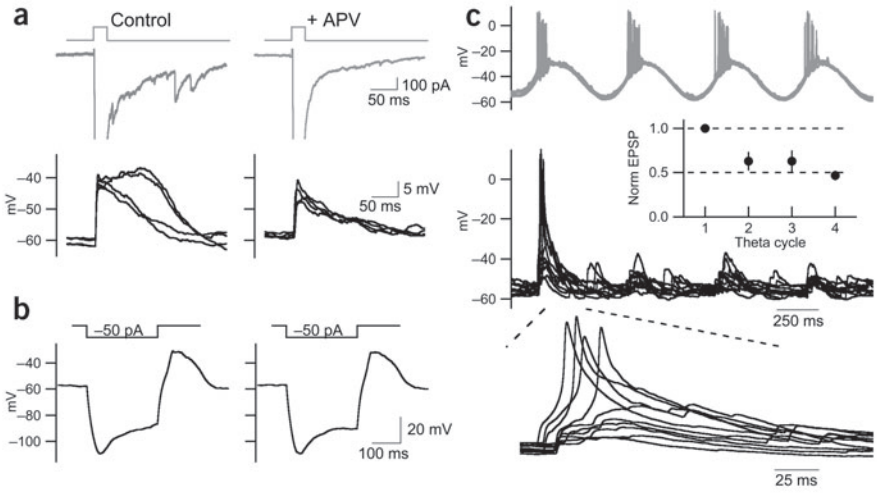

Figure 8 Dendritic glutamate release from a tufted cell generates an all-or-none Ca^{2+} spike in synaptically coupled periglomerular neurons. (**a**) In TTX, a brief voltage step to cause glutamate release from a tufted cell (gray traces) generates a large EPSP in the periglomerular neuron (black traces), which in turn leads to a Ca^{2+} spike in about half of the trials. The spike did not depend on the small (~3 mV) fluctuations in postsynaptic membrane potential. In the presence of APV (50 μM), glutamate release from the tufted cell still generated a large average EPSP in the periglomerular neuron, but no Ca^{2+} spike. Four consecutive trials of EPSPs are superimposed. (**b**) The rebound Ca^{2+} spike, which had a similar time course to the glutamate-evoked Ca^{2+} spike, was not affected by APV. (**c**) In current clamp, 2 Hz sinusoidal current injection evokes bursts of action potentials in a tufted cell (gray traces) that generate an all-or-none complex spike in a synaptically coupled periglomerular neuron (black traces) in 4 of 10 trials. The inset plots the normalized EPSP amplitude in periglomerular neurons versus the tufted cell theta cycle number ($n = 9$). Periglomerular traces are shown on an expanded timescale below.

Paired recordings revealed that dendritic release from one periglomerular neuron can mediate fast and slow $GABA_AR$-mediated responses in neighboring periglomerular neurons. Although GABA spillover or receptors with intrinsically slow kinetics may contribute to slow transmission, the kinetics of signaling between most periglomerular neurons was consistent with synaptic transmission. Anatomical studies have not reported evidence for dendrodendritic synapses formed between periglomerular neurons in mammals[1–3]. However, as pointed out previously[3], the complexity of dendritic processes in glomeruli can make it difficult to establish unequivocally the identity of pre- and postsynaptic cell types. Indeed, recent anatomical studies raise the possibility that calbindin-positive periglomerular neurons receive dendritic GABAergic input[41,42]. Our data provide evidence for synaptic signaling between periglomerular neurons in the mammalian olfactory bulb, and suggest a greater degree of synaptic complexity in glomerular circuits than was previously appreciated.

Pharmacological experiments have suggested that T-type Ca^{2+} channels may underlie GABA release from the dendrites of granule cells in the olfactory bulb[15]. We examined directly the nature of the Ca^{2+} channels governing transmitter release from periglomerular dendrites in paired recordings. Our results indicate that HVA Ca^{2+} currents are required for dendritic GABA release. Given the more extensive dendritic arbors of granule cells compared with periglomerular cells, it may be that granule cells use different mechanisms to trigger dendritic GABA release.

We found that single action potentials are far less effective at triggering transmitter release than dendritic Ca^{2+} spikes. Although some periglomerular cells have axons, these typically project into other glomeruli, where they may contribute to lateral inhibition[43]. We therefore think that the action potential–evoked release that we observed in periglomerular cell pairs in the same glomerulus reflects dendrodendritic transmission.

We found that low-threshold Ca^{2+} spikes in periglomerular cells do not seem to require T-type Ca^{2+} channels and that nimodipine, an antagonist of L-type channels, inhibits Ca^{2+} spikes. Although it has been reported that nimodipine can block T-type channels[32,44], the L-channel agonist Bay K 8644 recovered Ca^{2+} spikes in periglomerular cells. In agreement with a previous study[45], we found that that Ca^{2+} spikes are relatively insensitive to low concentrations (100 μM) of Ni^{2+} that typically block low-threshold Ca^{2+} spikes in other neurons[24]. At 1 mM, Ni^{2+} blocked Ca^{2+} spikes in periglomerular cells[45]; however, at this concentration Ni^{2+} acts as a broad-spectrum calcium channel blocker[32].

The simplest interpretation of our data is that LVA L-type channels have a critical role in generating periglomerular cell Ca^{2+} spikes. In support of this idea, we found that hyperpolarization caused a decrease in resting $[Ca^{2+}]$ in periglomerular dendrites. It is unlikely that T-type channels underlie a resting calcium conductance because they should be inactivated near the resting potential of periglomerular cells[24]. Although our voltage-clamp recordings did not reveal evidence for substantial T-type current, we did find rapidly activating, sustained LVA Ca^{2+} currents in periglomerular cells. Sustained LVA currents were partially blocked by nimodipine and enhanced by Bay K 8644. These results are consistent with other studies of neuronal LVA L-type currents[31,33,34]. Indeed, the expression of CaV1.3 channel subunits generates LVA L-type currents with similar properties[46,47]. Although we cannot rule out a contribution of T-type channels in some periglomerular cells, LVA L-channels seem sufficient for the generation of low-threshold Ca^{2+} spikes.

As reported previously[45], we found that prolonged hyperpolarization leads to a rebound Ca^{2+} spike in periglomerular cells. The deactivation and subsequent reactivation of LVA L-type channels at the resting membrane potential provides a simple mechanism for generation of rebound Ca^{2+} spikes in periglomerular cells. The high input resistance of periglomerular cells[20,39,45,48] makes it plausible that relatively small currents can have large effects on membrane potential. A high density of dendritic Ca^{2+} channels in periglomerular cells would be ideal for the initiation of a regenerative Ca^{2+} spike not unlike the regenerative nature of conventional action potentials.

Although L-type channels are required for tufted cell–periglomerular cell DDI, they do not directly contribute to glutamate or GABA release under normal conditions. We showed that blockers of P/Q-type Ca^{2+} channels inhibit GABA release from periglomerular dendrites. This is consistent with the high expression of P-type channels in periglomerular cells[49]. Residual release in the presence of toxins may reflect the contribution of R-type Ca^{2+} channels or difficulty in achieving saturating toxin concentrations in glomerular compartments. These data demonstrate separate roles (depolarization versus exocytosis) for different Ca^{2+} channel types that act in concert in periglomerular dendrites.

Why do Ca^{2+} spikes trigger dendritic GABA release more effectively than fast Na^+ spikes? We found that single action potentials cause Ca^{2+} transients throughout periglomerular cell dendrites, making it unlikely that action potentials do not propagate to dendritic release sites. One possibility is that the brief depolarization provided by action potentials is not coupled as effectively to the P/Q channels that underlie release. Indeed, the much slower Ca^{2+} spikes produce larger dendritic Ca^{2+} transients than trains of Na^+-dependent action potentials. In olfactory bulb granule cells, A-type K^+ channels specifically attenuate rapid dendritic excitation[50]. Similarly, we think it likely that active conductances in periglomerular dendrites limit the ability of short-duration (action potential–like) inputs to activate dendritic Ca^{2+} spikes and trigger release.

Glutamate release from a single tufted cell can have a large impact on synaptically coupled periglomerular neurons. We observed activation of approximately five periglomerular cells by single tufted cells. This suggests that the synchronous activation of many M/T neurons is not necessary to produce intraglomerular inhibition. Given that our slice experiments are carried out on cut segments of spherical glomeruli, the number of periglomerular cells activated by single tufted cells is likely to be much higher in intact glomeruli. The activation of periglomerular cell ensembles occurred with substantial temporal jitter. Our results support the idea that the slow time course of DDI reflects both the temporal variability in onset of periglomerular cell Ca^{2+} spikes and calcium buffer saturation in periglomerular dendrites.

Finally, our paired tufted cell–periglomerular cell recordings indicate that single tufted cells generate a powerful EPSP in glomerular interneurons. We showed that NMDARs facilitate dendritic Ca^{2+} spike generation in GABAergic interneurons. This is consistent with the idea that the crucial role of NMDARs in DDI reflects their intrinsically slow kinetics[14,50] rather than their Ca^{2+} permeability. We also found that activation of periglomerular neurons by principal neurons is dynamic and adapts rapidly during physiologically relevant (theta) activity. The marked depression of tufted cell EPSPs in periglomerular neurons after the first theta cycle may reflect the depletion of available transmitter from tufted cell dendritic release sites. This adaptation of periglomerular input is similar to that of odor-evoked lateral inhibition in M/T neurons and granule cell excitation *in vivo*[8], suggesting that adaptation may be a common feature of dendrodendritic transmission between principal neurons and interneurons in the bulb.

METHODS

Electrophysiology. Olfactory bulb slices (~250–300 μm) were prepared from 2–4-week-old Sprague-Dawley rats in accordance with institutional and national guidelines using standard procedures. Slices were prepared and maintained in aCSF containing 83 mM NaCl, 2.5 mM KCl, 3.3 mM $MgSO_4$, 1 mM NaH_2PO_4, 26.2 mM $NaHCO_3$, 22 mM glucose, 72 mM sucrose and 0.5 mM $CaCl_2$, and equilibrated with 95% O_2/5% CO_2 at 34 °C for 15–30 min and at room temperature thereafter. In the recording chamber, slices were viewed by means of infrared-DIC optics (BX-51W1, Olympus) and superfused with aCSF containing 119 mM NaCl, 2.5 mM KCl, 1.3 mM $MgSO_4$, 1 mM NaH_2PO_4, 26.2 mM $NaHCO_3$, 22 mM glucose and 2.5 mM $CaCl_2$.

Whole-cell electrodes (~3–4 MΩ) for voltage-clamp recordings were filled with a solution containing 120 mM CsCl, 10 mM TEA-Cl, 10 mM HEPES, 12 mM phosphocreatine, 0.25–10 mM EGTA, 3 mM Mg-ATP, 0.2 mM Na-GTP and 10 mM GABA (pH ~7.35, 300 mOsm). For isolating calcium currents, Cs-gluconate replaced CsCl in the internal solution and the aCSF included 100 μM picrotoxin, 1 μM TTX, 1 mM 4-aminopyridine, 4 mM TEA and 5 mM CsCl. The holding potential was –70 mV unless otherwise noted. For tufted cell recordings, glutamate replaced GABA in the internal solution. Current-clamp recordings were carried out with a KCH_3SO_4-based internal solution containing 115.5 KCH_3SO_4, 17.5 mM KCl, 10 mM HEPES, 10 mM phosphocreatine, 3 mM magnesium ATP, 0.2 mM sodium GTP, 0.5 mM EGTA and 10 mM GABA (pH ~7.35, 300 mOsm). This internal solution mimics the Cl^- reversal potential (–50 mV) previously measured in periglomerular cells[20].

Series resistance was typically <10 MΩ and compensated by ≥90%. Experiments using cesium gluconate– or KCH_3SO_4-based internal solutions were corrected for a 10 mV junction potential. Responses were recorded with Axopatch 200B amplifiers (Axon Instruments), filtered at 2–5 KHz and digitized at 10–20 KHz (ITC-18; Instrutech). Data acquisition and analysis were performed with Axograph 4.8 (Axon) and IGOR Pro 4 (Wavemetrics). Experiments examining periglomerular cell–periglomerular cell signaling were carried out in the presence of CGP 55845 or CGP 54626 (2.5–5 μM) and 1,2,3,4-tetrahydro-6-nitro-2,3-dioxo-benzo[f]quinoxaline-7-sulfonamide (NBQX) to block $GABA_B$ and AMPA receptors, respectively. Experiments were carried out at 31–33 °C unless otherwise noted. Ca^{2+} currents were determined using leak subtraction (P/4). Experiments examining Ca^{2+} currents and the voltage dependence of release were carried out at room temperature.

Imaging. For Ca^{2+} imaging of periglomerular dendrites Oregon Green-1 (100 μM; Molecular Probes) replaced EGTA in the internal solution. Image acquisition (494 nm excitation, 2 × 2 binning, 25–50 Hz) and analysis were carried out with a cooled-CCD camera system (T.I.L.L. Photonics). Regions of interest for analysis were restricted to portions of dendrite in the focal plane.

To examine network properties of tufted cell and periglomerular cells, slices were loaded with Oregon Green-1 AM (10 μM, with 0.02% Pluronic F-127) at 34 °C for 30 min. We observed preferential labeling of periglomerular cells relative to principal neurons in the glomerular layer. Tufted cells were filled intracellularly with Alexa 568 (10 μM; Molecular Probes). Calcium transients were imaged at 494 nm excitation (30 Hz, 4 × 4 binning) and tufted cell images were acquired at 568 nm. Regions of interest (~10 μm diameter) centered over periglomerular somata were used for kinetic analysis.

Representative traces are the average of five or more consecutive episodes, except where noted. Data are presented as mean ± s.e.m. Student's *t*-test was used to determine statistical significance.

Note: Supplementary information is available on the Nature Neuroscience website.

ACKNOWLEDGMENTS

We thank M. Scanziani, P. Sah and K. Franks for helpful discussions. G.J.M. received support from an NRSA predoctoral fellowship (NIDCD; DC005679). J.S.I. received support from a McKnight Scholar Award, Klingenstein Award, Burroughs-Wellcome Career Award and the NIH (RO1 DC04682).

COMPETING INTERESTS STATEMENT

The authors declare that they have no competing financial interests.

Received 22 December 2004; accepted 14 January 2005
Published online at http://www.nature.com/natureneuroscience/

1. White, E.L. Synaptic organization of the mammalian olfactory glomerulus: new findings including an intraspecific variation. *Brain Res.* **60**, 299–313 (1973).
2. White, E.L. Synaptic organization in the olfactory glomerulus of the mouse. *Brain Res.* **37**, 69–80 (1972).
3. Pinching, A.J. & Powell, T.P. The neuropil of the glomeruli of the olfactory bulb. *J. Cell Sci.* **9**, 347–377 (1971).
4. Shepherd, G.M. & Greer, C.A. Olfactory bulb. in *The Synaptic Organization of the Brain* (ed. Shepherd, G.M.) 159–203 (Oxford Univ. Press, Oxford, 1998).
5. Brennan, P.A. & Keverne, E.B. Neural mechanisms of mammalian olfactory learning. *Prog. Neurobiol.* **51**, 457–481 (1997).
6. Yokoi, M., Mori, K. & Nakanishi, S. Refinement of odor molecule tuning by dendrodendritic synaptic inhibition in the olfactory bulb. *Proc. Natl Acad. Sci. USA* **92**, 3371–3375 (1995).
7. Spors, H. & Grinvald, A. Spatio-temporal dynamics of odor representations in the mammalian olfactory bulb. *Neuron* **34**, 301–315 (2002).
8. Cang, J. & Isaacson, J.S. *In vivo* whole-cell recording of odor-evoked synaptic transmission in the rat olfactory bulb. *J. Neurosci.* **23**, 4108–4116 (2003).
9. Margrie, T.W. & Schaefer, A.T. Theta oscillation coupled spike latencies yield computational vigour in a mammalian sensory system. *J. Physiol. (Lond.)* **546**, 363–374 (2003).
10. Isaacson, J.S. & Strowbridge, B.W. Olfactory reciprocal synapses: dendritic signaling in the CNS. *Neuron* **20**, 749–761 (1998).
11. Chen, W.R., Xiong, W. & Shepherd, G.M. Analysis of relations between NMDA receptors and GABA release at olfactory bulb reciprocal synapses. *Neuron* **25**, 625–633 (2000).
12. Schoppa, N.E., Kinzie, J.M., Sahara, Y., Segerson, T.P. & Westbrook, G.L. Dendrodendritic inhibition in the olfactory bulb is driven by NMDA receptors. *J. Neurosci.* **18**, 6790–6802 (1998).
13. Halabisky, B., Friedman, D., Radojicic, M. & Strowbridge, B.W. Calcium influx through NMDA receptors directly evokes GABA release in olfactory bulb granule cells. *J. Neurosci.* **20**, 5124–5134 (2000).
14. Isaacson, J.S. Mechanisms governing dendritic γ-aminobutyric acid (GABA) release in the rat olfactory bulb. *Proc. Natl Acad. Sci. USA* **98**, 337–342 (2001).
15. Egger, V., Svoboda, K. & Mainen, Z.F. Mechanisms of lateral inhibition in the olfactory bulb: efficiency and modulation of spike-evoked calcium influx into granule cells. *J. Neurosci.* **23**, 7551–7558 (2003).
16. Price, J.L. & Powell, T.P. The synaptology of the granule cells of the olfactory bulb. *J. Cell Sci.* **7**, 125–155 (1970).
17. Christie, J.M., Schoppa, N.E. & Westbrook, G.L. Tufted cell dendrodendritic inhibition in the olfactory bulb is dependent on NMDA receptor activity. *J. Neurophysiol.* **85**, 169–173 (2001).
18. Aroniadou-Anderjaska, V., Zhou, F.M., Priest, C.A., Ennis, M. & Shipley, M.T. Tonic and synaptically evoked presynaptic inhibition of sensory input to the rat olfactory bulb via $GABA_B$ heteroreceptors. *J. Neurophysiol.* **84**, 1194–1203 (2000).
19. Murphy, G.J., Glickfeld, L.L., Balsen, Z. & Isaacson, J.S. Sensory neuron signaling to the brain: properties of transmitter release from olfactory nerve terminals. *J. Neurosci.* **24**, 3023–3030 (2004).
20. Smith, T.C. & Jahr, C.E. Self-inhibition of olfactory bulb neurons. *Nat. Neurosci.* **5**, 760–766 (2002).
21. Salin, P.A. & Prince, D.A. Spontaneous $GABA_A$ receptor-mediated inhibitory currents in adult rat somatosensory cortex. *J. Neurophysiol.* **75**, 1573–1588 (1996).
22. Hausser, M. & Roth, A. Estimating the time course of the excitatory synaptic conductance in neocortical pyramidal cells using a novel voltage jump method. *J. Neurosci.* **17**, 7606–7625 (1997).
23. Pearce, R.A. Physiological evidence for two distinct $GABA_A$ responses in rat hippocampus. *Neuron* **10**, 189–200 (1993).
24. Perez-Reyes, E. Molecular physiology of low-voltage-activated t-type calcium channels. *Physiol. Rev.* **83**, 117–161 (2003).
25. Holderith, N.B., Shigemoto, R. & Nusser, Z. Cell type-dependent expression of HCN1 in the main olfactory bulb. *Eur. J. Neurosci.* **18**, 344–354 (2003).
26. Cadetti, L. & Belluzzi, O. Hyperpolarisation-activated current in glomerular cells of the rat olfactory bulb. *Neuroreport* **12**, 3117–3120 (2001).
27. Regehr, W., Kehoe, J.S., Ascher, P. & Armstrong, C. Synaptically triggered action potentials in dendrites. *Neuron* **11**, 145–151 (1993).
28. Golding, N.L. & Spruston, N. Dendritic sodium spikes are variable triggers of axonal action potentials in hippocampal CA1 pyramidal neurons. *Neuron* **21**, 1189–1200 (1998).
29. Kim, H.G. & Connors, B.W. Apical dendrites of the neocortex: correlation between sodium- and calcium-dependent spiking and pyramidal cell morphology. *J. Neurosci.* **13**, 5301–5311 (1993).
30. Schwindt, P. & Crill, W. Equivalence of amplified current flowing from dendrite to soma measured by alteration of repetitive firing and by voltage clamp in layer 5 pyramidal neurons. *J. Neurophysiol.* **76**, 3731–3739 (1996).
31. Pennartz, C.M., de Jeu, M.T., Bos, N.P., Schaap, J. & Geurtsen, A.M. Diurnal modulation of pacemaker potentials and calcium current in the mammalian circadian clock. *Nature* **416**, 286–290 (2002).
32. Avery, R.B. & Johnston, D. Multiple channel types contribute to the low-voltage-activated calcium current in hippocampal CA3 pyramidal neurons. *J. Neurosci.* **16**, 5567–5582 (1996).
33. Magee, J.C., Avery, R.B., Christie, B.R. & Johnston, D. Dihydropyridine-sensitive, voltage-gated Ca^{2+} channels contribute to the resting intracellular Ca^{2+} concentration of hippocampal CA1 pyramidal neurons. *J. Neurophysiol.* **76**, 3460–3470 (1996).
34. Power, J.M. & Sah, P. Intracellular calcium store filling by an L-type calcium current in the basolateral amygdala at subthreshold membrane potentials. *J. Physiol.* **562**, 439–453 (2005).
35. Salin, P.A., Lledo, P.M., Vincent, J.D. & Charpak, S. Dendritic glutamate autoreceptors modulate signal processing in rat mitral cells. *J. Neurophysiol.* **85**, 1275–1282 (2001).
36. Friedman, D. & Strowbridge, B.W. Functional role of NMDA autoreceptors in olfactory mitral cells. *J. Neurophysiol.* **84**, 39–50 (2000).
37. Isaacson, J.S. Glutamate spillover mediates excitatory transmission in the rat olfactory bulb. *Neuron* **23**, 377–384 (1999).
38. Macrides, F. & Chorover, S.L. Olfactory bulb units: activity correlated with inhalation cycles and odor quality. *Science* **175**, 84–87 (1972).
39. Hayar, A., Karnup, S., Shipley, M.T. & Ennis, M. Olfactory bulb glomeruli: external tufted cells intrinsically burst at theta frequency and are entrained by patterned olfactory input. *J. Neurosci.* **24**, 1190–1199 (2004).
40. Schoppa, N.E. & Westbrook, G.L. Glomerulus-specific synchronization of mitral cells in the olfactory bulb. *Neuron* **31**, 639–651 (2001).
41. Toida, K., Kosaka, K., Heizmann, C.W. & Kosaka, T. Chemically defined neuron groups and their subpopulations in the glomerular layer of the rat main olfactory bulb: III. Structural features of calbindin D28K-immunoreactive neurons. *J. Comp. Neurol.* **392**, 179–198 (1998).
42. Kosaka, K., Toida, K., Aika, Y. & Kosaka, T. How simple is the organization of the olfactory glomerulus? The heterogeneity of so-called periglomerular cells. *Neurosci. Res.* **30**, 101–110 (1998).
43. Aungst, J.L. *et al.* Centre-surround inhibition among olfactory bulb glomeruli. *Nature* **426**, 623–629 (2003).
44. Stengel, W., Jainz, M. & Andreas, K. Different potencies of dihydropyridine derivatives in blocking T-type but not L-type Ca^{2+} channels in neuroblastoma-glioma hybrid cells. *Eur. J. Pharmacol.* **342**, 339–345 (1998).
45. McQuiston, A.R. & Katz, L.C. Electrophysiology of interneurons in the glomerular layer of the rat olfactory bulb. *J. Neurophysiol.* **86**, 1899–1907 (2001).
46. Lipscombe, D., Helton, T.D. & Xu, W. L-type calcium channels: the low down. *J. Neurophysiol.* **92**, 2633–2641 (2004).
47. Xu, W. & Lipscombe, D. Neuronal $Ca_V1.3\alpha_1$ L-type channels activate at relatively hyperpolarized membrane potentials and are incompletely inhibited by dihydropyridines. *J. Neurosci.* **21**, 5944–5951 (2001).
48. Puopolo, M. & Belluzzi, O. Functional heterogeneity of periglomerular cells in the rat olfactory bulb. *Eur. J. Neurosci.* **10**, 1073–1083 (1998).
49. Hillman, D. *et al.* Localization of P-type calcium channels in the central nervous system. *Proc. Natl Acad. Sci. USA* **88**, 7076–7080 (1991).
50. Schoppa, N.E. & Westbrook, G.L. Regulation of synaptic timing in the olfactory bulb by an A-type potassium current. *Nat. Neurosci.* **2**, 1106–1113 (1999).